Empirical Dust Models

ChangHoon Hahn[1, 2, *] and IQ Collaboratory

[1]*Lawrence Berkeley National Laboratory, 1 Cyclotron Rd, Berkeley CA 94720, USA*
[2]*Berkeley Center for Cosmological Physics, University of California, Berkeley CA 94720, USA*

(Dated: `DRAFT --- 85405b7 --- 2020-06-05 --- NOT READY FOR DISTRIBUTION`)

ABSTRACT

dust

Keywords: keyword1 – keyword2 – keyword3

1. INTRODUCTION

dust is important because....

assumptions on the attenuation curve can dramatically impact the physical properties inferred from SED fitting (*e.g.* Kriek & Conroy 2013; **?**; **?**; Salim & Narayanan 2020).

motivation for an empirical dust attenuation model

attenuation vs extinction. While extinction curves have been derived from observations and theoretically, it's not easy to map this to attenuation curves. Attenuation curves are a product of complicated empirical processes since it accounts for light that gets scattered and star light that is not obscured

This makes modeling them in a complete physically motivated method expensive. People have done it Narayanan et al. (2018); Trayford et al. (2020). some detail about the radiative transfer method and such. But besides being expensive they have to make a number of assumptions anyway. e.g. Narayanan et al. (2018) assumes a fixed extinction curve.

Moreover, because the radiative transfer method is expensive it's hard to compare many different simulations. Not only that, observables generated from simulations that take into radative transfer dust models complicates simulation to simulation comparisons. Because you're simultaneously comparing the galaxy formation prescription and all the dust prescription.

Instead, we present a framework using flexible dust empirical models that paints attenuation curves onto galaxies. describe at a high level how we are parameterizing DEMs

talk about the advantages: extremely flexible so it can encompass the wide variety of attenuation curves found in radiative transfer, easy to correlate the attenuation curve with galaxy properties.

Also DEMs make it possible to statistically apply attenuation curves for large galaxy population. Putting this ontop of simulations, we can use them to generate observables and compare them to
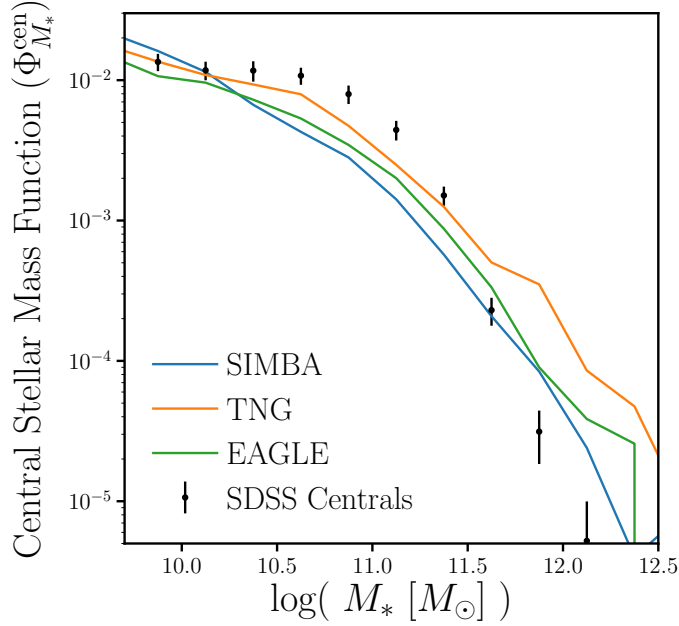
* hahn.changhoon@gmail.com

Figure 1. The stellar mass functions of central galaxies, $\Phi_{M_*}^{\mathrm{cen}}$, of the SIMBA (orange) and TNG (blue) simulations compared to the SDSS $\Phi_{M_*}^{\mathrm{cen}}$. The uncertainties for the SDSS $\Phi_{M_*}^{\mathrm{cen}}$ are derived using jackknife resampling and SDSS centrals are identified using a halo-based group finder (Section 2.1). For SIMBA and TNG galaxies, we calculate M_* as the total stellar mass within the host halo, excluding contributions from any subhalos; centrals are classified based on their individual definition (Section 2.2 and 2.3). *should we include total SMF...? The simulations and observations have loosely consistent* $\Phi_{M_*}^{\mathrm{cen}}$.

observations to constrain the DEM. This framework allows us to learn about attenuation curves given a model for galaxy formation.

The other way around also works. If you don't care about dust at all, DEM provides a framework to easily marginalize over dust attenuation and treat dust as a nuisance parameter.

In this paper, we do above for multiple simulations.

Starkenburg et la. in prep will use this framework to marginalize over dust and compare galaxy populations predicted by multiple simulations .

2. DATA

2.1. *SDSS DR7 Central Galaxies*

Throughout the paper we compare the simulations and models described below to the observed SDSS central galaxy sample from the Tinker et al. (2011) group catalog. The group catalog, first, selects volume-limited sample of galaxies at $z \approx 0.04$ with $M_r < -18$ and complete above $M_* > 10^{9.4}h^{-2}M_{\odot}$ from the NYU Value-Added Galaxy Catalog (VAGC; Blanton et al. 2005) of SDSS DR7 (Abazajian et al. 2009). The stellar masses are estimated using the `kcorrect` code (Blanton & Roweis 2007) assuming a Chabrier (2003) initial mass function.

Central galaxies are then identified using a halo-based group finder that uses the abundance matching ansatz to iteratively assign halo masses to groups. Every group contains one central galaxy,

which by definition is the most massive, and a group can contain ≥ 0 satellites. As with any group finder, galaxies are misassigned due to projection effects and redshift space distortions; however, the central galaxy sample has a purity of $\sim 90\%$ and completeness of $\sim 95\%$ (Tinker et al. 2018).

2.2. *Illustris TNG*

describe what galaxy properties (SFH, ZH, etc) are available

TODO

2.3. *SIMBA*

describe what galaxy properties (SFH, ZH, etc) are available

TODO

In Figure 1, we compare the stellar mass function (SMF) of our SDSS central galaxy sample along with central galaxy SMFs of the SIMBA (orange) and TNG (blue) simulations. The uncertainties for the SDSS SMF are derived from jackknife resampling. Although we present the SMFs for reference, we do not use stellar masses throughout the paper since they are inconsistently defined among simulations and observations. Instead, we compare between the simulations and SDSS using luminosity, M_r, which we consistently forward model and measure in the simulations. In these comparisons, we restrict ourselves to galaxies brighter than $M_r < -20$, where our SDSS central galaxy sample is complete.

instantaneous SFR=0 for $\sim 11\%$ of SIMBA galaxies, $\sim 13\%$ for TNG, $\sim 2\%$ for EAGLE

2.4. *Spectral Energy Distributions*

describe how the SED is generated using the SFH and ZHs

TODO

2.5. *Forward Modeling SDSS Photometry and Spectra*

3. DUST EMPIRICAL MODELING

3.1. *Fiducial DEM*

motivation for the DEM model

TODO

We begin by defining the dust attenuation curve $A(\lambda)$ as

$$F_o(\lambda) = F_i(\lambda)10^{-0.4A(\lambda)} \tag{1}$$

where F_o is the observed flux and F_i is the intrinsic flux. We normalize the attenuation at the V band,

$$A(\lambda) = A_V \frac{k(\lambda)}{k_V}. \tag{2}$$

For the normalization of the attenuation curve, A_V, we use the slab model from Somerville & Primack (1999); Somerville et al. (2012). In the slab model the amplitude of attuenuation depends on the inclination angle, i, and the optical depth, τ_V:

$$A_V = -2.5\log\left[\frac{1 - e^{-\tau_V \sec i}}{\tau_V \sec i}\right] \tag{3}$$

justification of why this is enough. We sample i uniformly.
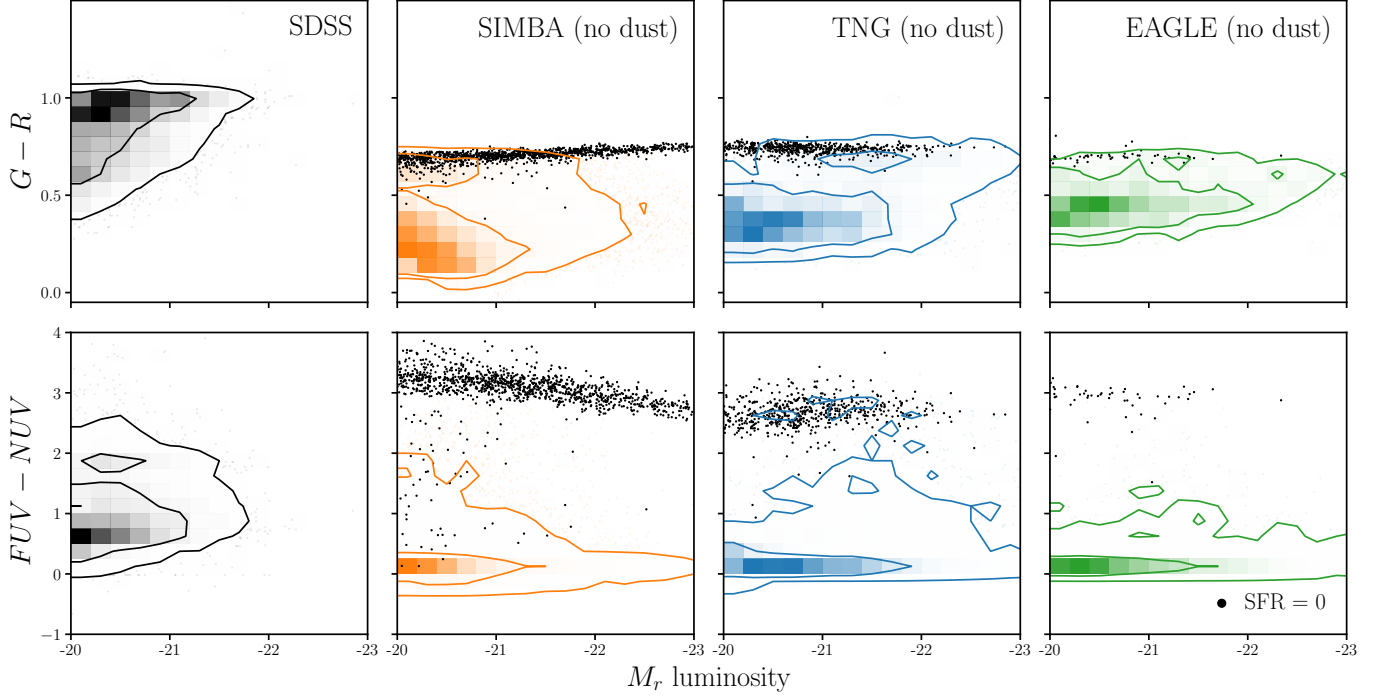
TODO

Figure 2. We present the distributions of the main observables used throughout the paper for SDSS (left), SIMBA (center), and TNG (right) centrals. We do *not* include any prescription for dust for the simulated galaxies. The top panels present the $G - R$ versus M_r color magnitude relations while the bottom panels present the $FUV - NUV$ versus M_r relations. The observables for the SIMBA and TNG simulated galaxies are derived using forward modeling and are therefore consistent with SDSS measurements (Section 2.5). The contours for SIMBA and TNG do not include galaxies with SFR$= 0$, which we mark separately in black. Despite similar SMFs, *the simulations without any dust prescription show stark differences with observations in the color-magnitude observable-space.*

Recently, Salim & Narayanan (2020) find significant dependence in A_V on both M_* and SFR. We include this dependence through τ_V, which we flexibly parameterize as

$$\tau_V(M_*, \mathrm{SFR}) = m_{\tau,1} \log\left(\frac{M_*}{10^{10} M_\odot}\right) + m_{\tau,2} \log \mathrm{SFR} + c_\tau. \tag{4}$$

Next, for the wavelength dependence of the attenuation curve, we use $k(\lambda)$ from Noll et al. (2009):

$$k(\lambda) = (k_{\mathrm{Cal}}(\lambda) + D(\lambda))\left(\frac{\lambda}{\lambda_V}\right)^\delta. \tag{5}$$

Here $k_{\mathrm{Cal}}(\lambda)$ is the Calzetti (2001) curve:

$$k_{\mathrm{Cal}}(\lambda) = \begin{cases} 2.659(-1.857 + 1.040/\lambda) + R_V, & 6300 \mathring{A} \leq \lambda \leq 22000 \mathring{A} \\ 2.659(-2.156 + 1.509/\lambda - 0.198/\lambda^2 + 0.011/\lambda^3) + R_V & 1200 \mathring{A} \leq \lambda \leq 6300 \mathring{A} \end{cases}$$

where λ_V is the V band wavelength. δ, the slope of the attenuation curve. also correlates with galaxy properties. So we parameterize δ and

$$\delta(M_*, \mathrm{SFR}) = m_{\delta,2} \log\left(\frac{M_*}{10^{10} M_\odot}\right) + m_{\delta,2} \log \mathrm{SFR} + c_\delta \tag{6}$$

$D(\lambda)$ is the UV dust bump, which we parameter using the standard Lorentzian-like Drude profile:

$$D(\lambda) = \frac{E_b (\lambda \Delta\lambda)^2}{(\lambda^2 - \lambda_0^2)^2 + (\lambda \Delta\lambda)^2} \tag{7}$$

where λ_0, $\Delta\lambda$, and E_b are the central wavelength, FWHM, and strength of the bump, respecitvely. In our DEM, we assume fixed $\lambda_0 = 2175\mathring{A}$ and $\Delta\lambda = 350\mathring{A}$.

Kriek & Conroy (2013) and Tress et al. (2018) found evidence that E_b correlates with the slope of the attenuation curve for star-forming galaxies $z \sim 2$. This was dependence was confirmed with simulations in ?. E_b:

$$E_b = m_E \; \delta + c_E \tag{8}$$

We also split the attenuation on the star light and nebular emission

$$F_o(\lambda) = F_i^{\mathrm{star}}(\lambda) 10^{-0.4 A(\lambda)} + F_i^{\mathrm{neb}}(\lambda) 10^{-0.4 A_{\mathrm{neb}}(\lambda)} \tag{9}$$

where we parameterize

$$A_{\mathrm{neb}}(\lambda) = f_{\mathrm{neb}} A(\lambda) \tag{10}$$

mention of how we treat SFR $= 0$ galaxies   TODO

3.2. Likelihood-Free Inference

Approximate Bayesian Computation with Population Monte Carlo Hahn et al. (2017),

To compare the outputs of our DEMs to observations, we first measure the color-magnitude observables ($G-R$, $FUV-NUV$, and M_r) as described in Section 2.5 consistent with SDSS measurements. Afterwards, we compare the forward modeled observables to SDSS using a L2 norm distance metric:

$$\bar{\rho}(\theta) = \sum_{i=1}^n \left[X_i^{\mathrm{SDSS}} - X_i^{\mathrm{model}}(\theta) \right]^2. \tag{11}$$

X^{SDSS} and $X^{\mathrm{model}}(\theta)$ are n-dimensional data vectors of the SDSS and model observables. In our case, we use a 3-dimensional histogram along $G-R$, $FUV-NUV$,

Ishida et al. (2015)

Paragraph on the priors we choose.

- flat priors on everything. We might want to note that this doesn't give flat priors on τ_V or μ_{A_V} and σ_{A_V} for NT but we're ultimately interested in the dependence.

- priors were chosen to be uninformative and encompass constraints in the literature:

- m_E and c_E were chosen to be include Kriek & Conroy (2013); Narayanan et al. (2018); Tress et al. (2018)
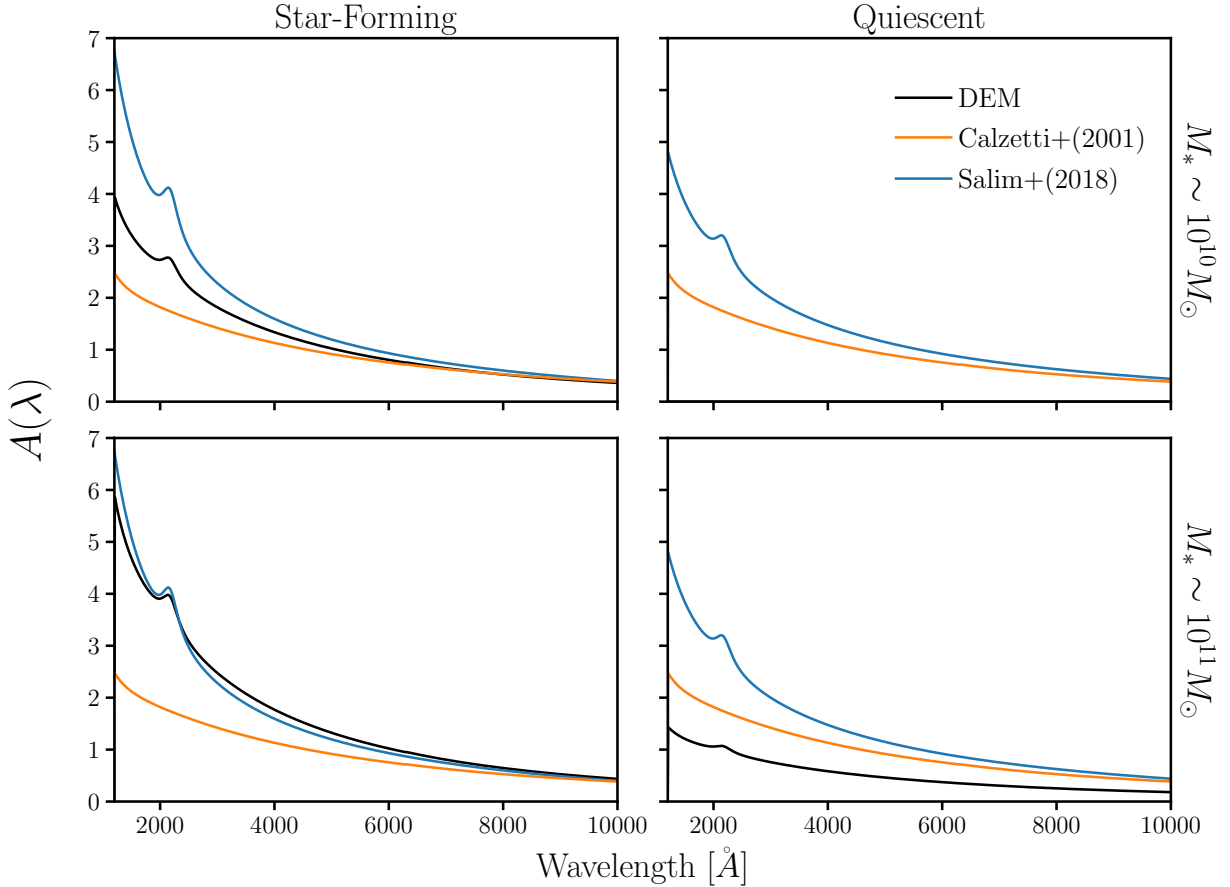
Figure 3. Comparison of the attenuation curve for our fiducial dust empirical model (DEM; black) to common attenuation curves in the literature (Calzetti 2001, orange; Salim et al. 2018, blue). We compare the curves for typical star-forming galaxies with SFR $= 10^{0.5} M_\odot/yr$ in the left panel and for quiescent galaxies with SFR $= 10^{-2} M_\odot/yr$ in the right. For our fiducial DEM, we use parameter values at the center of the priors listed in Table 1 and include attenuation curves for $M_* = 10^{9.5}$ (dashed) and $10^{11} M_\odot$ (solid). *Our fiducial DEM is flexibly parameterized to incorporate both M_* and SFR dependence in the attenuation curve* (Section 3.1).

4. RESULTS

- There isn't a whole lot of flexibility for SFR=0 galaxies predicted by simulations and they do not agree well with observations A.

5. SUMMARY

ACKNOWLEDGEMENTS

Table 1. Parameters of the Dust Empirical Models

Parameter	Definition	prior
	DEM with slab model	
$m_{\tau,1}$	Slope of the $\log M_*$ dependence of optical depth, τ_V	flat $[-5.,5.]$
$m_{\tau,2}$	Slope of the $\log \mathrm{SFR}$ dependence of optical depth, τ_V	flat $[-5.,5.]$
c_τ	amplitude of the optical depth, τ_V	flat $[0.,6.]$
	DEM with $\mathcal{N}_T$ model	
$m_{\mu,1}$	Slope of the $\log M_*$ dependence of optical depth, τ_V	flat $[-5.,5.]$
$m_{\mu,2}$	Slope of the $\log \mathrm{SFR}$ dependence of optical depth, τ_V	flat $[-5.,5.]$
c_μ	amplitude of the optical depth, τ_V	flat $[0.,6.]$
$m_{\sigma,1}$	Slope of the $\log M_*$ dependence of optical depth, τ_V	flat $[-5.,5.]$
$m_{\sigma,2}$	Slope of the $\log \mathrm{SFR}$ dependence of optical depth, τ_V	flat $[-5.,5.]$
c_σ	amplitude of the optical depth, τ_V	flat $[0.1,3.]$
$m_{\delta,1}$	Slope of the $\log M_*$ dependence of the attenuation curve slope, δ	flat $[-4.,4.]$
$m_{\delta,2}$	Slope of the $\log \mathrm{SFR}$ dependence of the attenuation curve slope, δ	flat $[-4.,4.]$
c_δ	amplitude of the attenuation curve slope, δ	flat $[-4.,4.]$
m_E	slope of the δ dependence of UV dust bump strength, E_b	flat $[-4.,0.]$
c_E	amplitude of UV dust bump strength, δ	flat $[0.,4.]$
f_{neb}	fraction of nebular attenuation curve	flat $[1.,4.]$

APPENDIX

A. RESOLUTION EFFECTS

Figure demonstrating imprint SFR=0 leave on the observable space and how we deal with them so we can ignore them...

B. BEYOND THE SLAB DEM

A major assumption of our fiducial DEM is that we sample the amplitude of attenuation from the slab model. The slab model makes the simplifying assumption that dust in galaxies are in a slab-like geometry and illuminated by the stellar radiation source (Somerville & Primack 1999). Then, for a given τ_V, the attenuation depends solely on the orientation of the galaxy. This simplification, ignores any complexities in the star-to-dust geometry that impact the shape of the attenuation curve (Witt Gordon 1996, 2000, Seon Drain 2016). TODO

Besides its simplifications, the slab model predicts A_V distribution with significant differences than the A_V distributions measured from observations. In Figure 11, we compare the A_V distribution predicted by the slab model (black) to the A_V distribution of star-forming galaxies in our SDSS
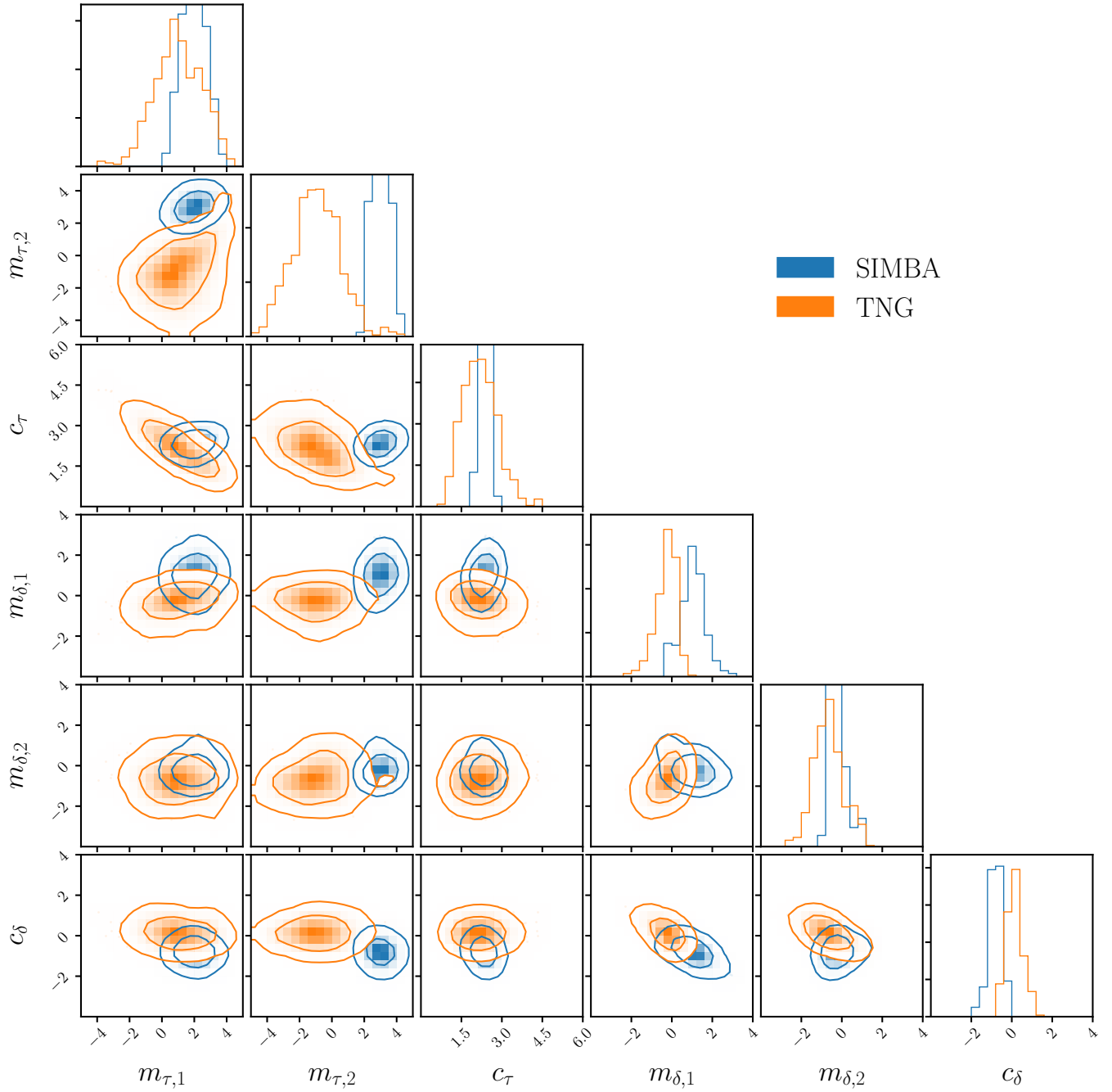
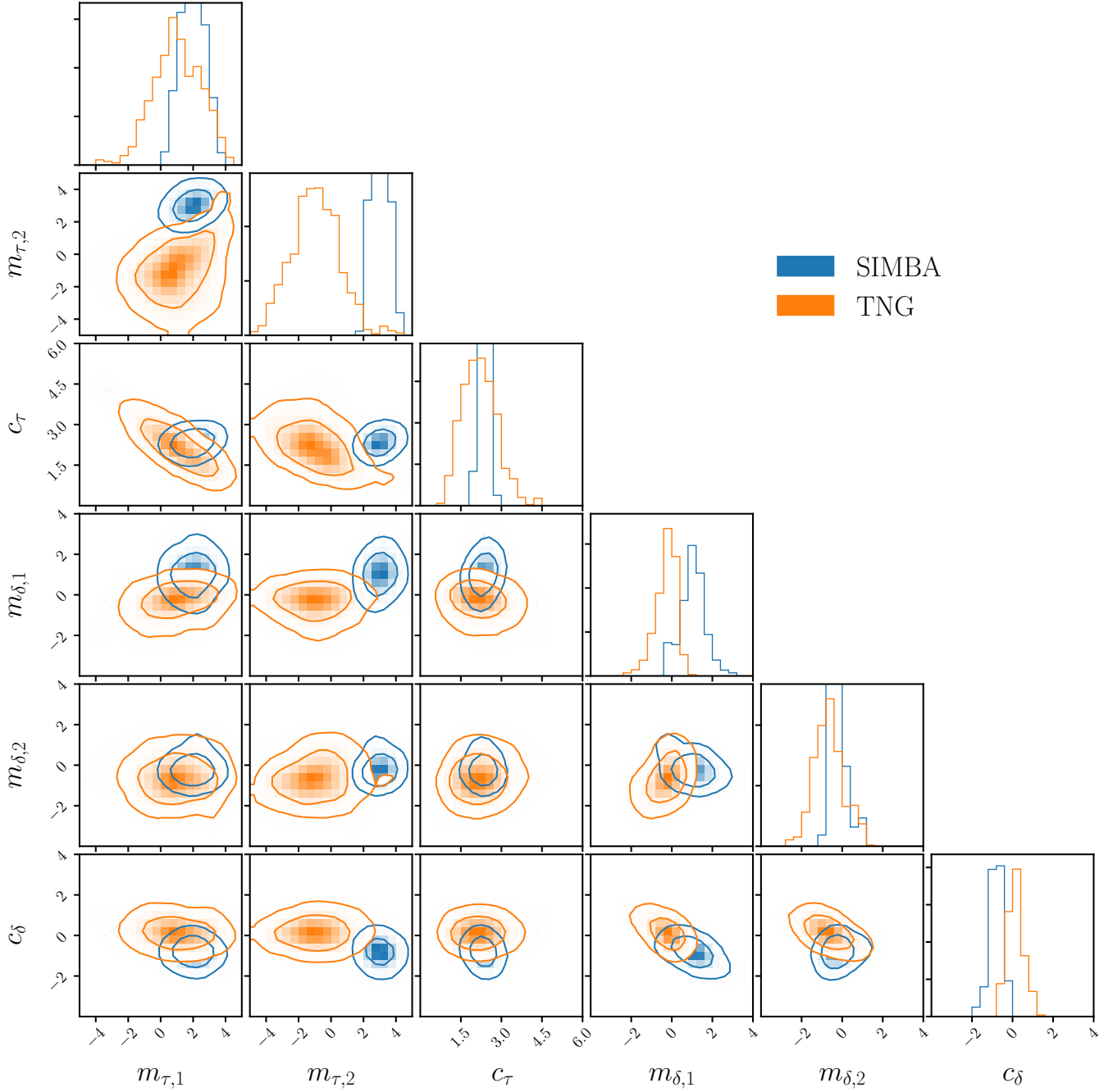**Figure 4.** Posterior distribution of our fidicuail DEM parameters derived using Approximate Bayesian Computation (ABC). (Section 3.2)

sample (blue). The A_V values are derived using SED fitting from the **?** MPA-JHU catalog and how are the SF galaxies classified. The slab model A_V values are derived using Eq. 3 and 4 with M_*s and SFRs from the same SDSS sample and the inclinations, i, are uniformly sampled over the range $[0, \pi/2]$. With $\{m_{\tau,1}, m_{\tau,2}, c_\tau\}$ chosen to reproduce the observed A_V distribution, the slab model can reproduce the overall shape. However, it predicts an extended high A_V tail not found in observations.

Figure 5. Posterior distribution of our fidicuail DEM parameters derived using Approximate Bayesian Computation (ABC). (Section 3.2)

Given these shortcomings of the slab model, we want to ensure that our results do not hinge on the slab model. Modeling the star-to-dust geometries with increased complexities, however, would involve expensive hydrodynamic simulations and dust radiative transfer calculations (*e.g.* Narayanan et al. 2018)jonsson2006, rocha2008, natale2015,hayward smith2015,hou2017,trayford2020. We instead take an empirical approach and implement a flexible model for sampling A_V based on a truncated normal

TODO
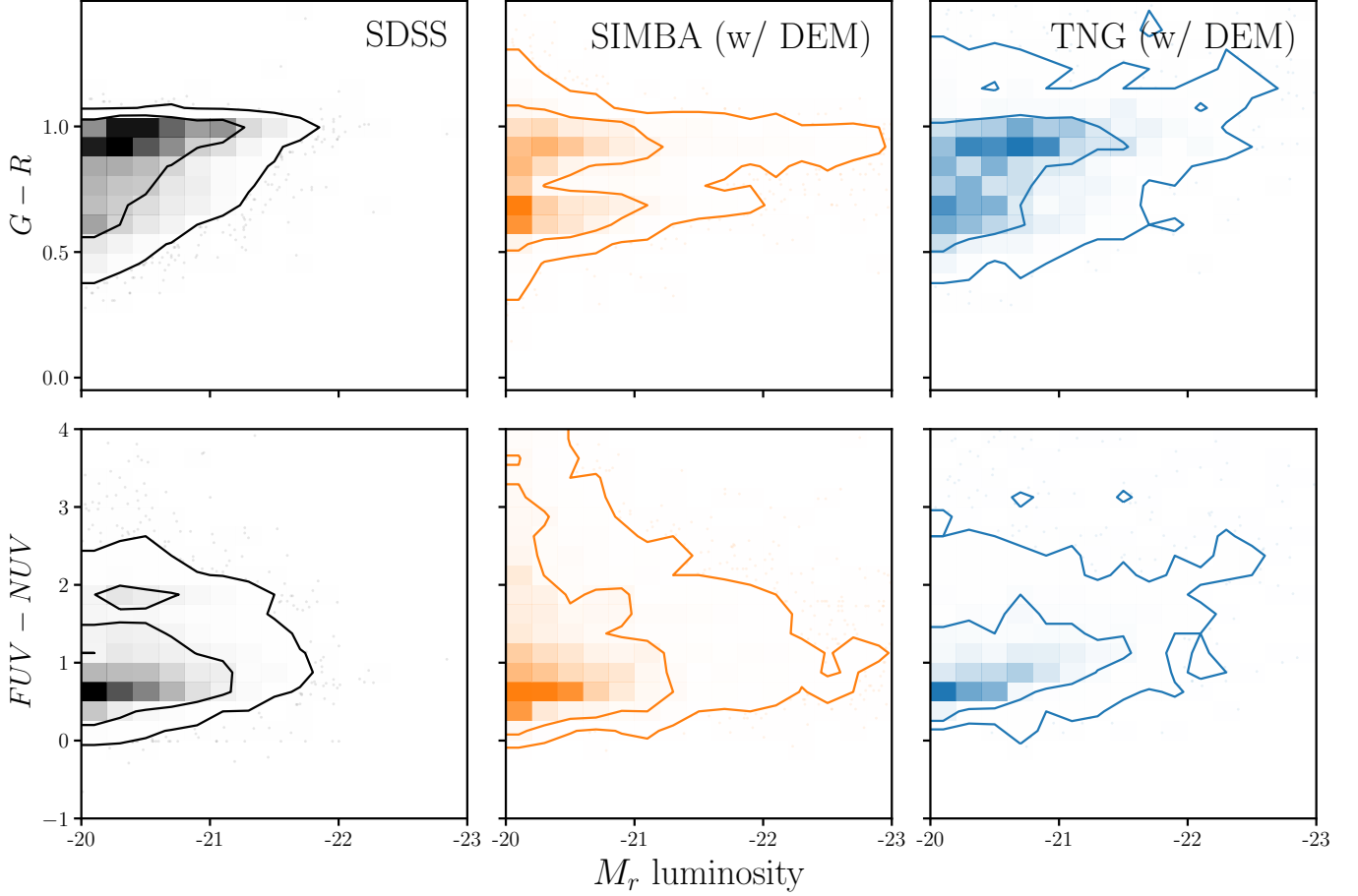
Figure 6. Comparison of the observables predicted by the simulations with the posterior DEM.

distribution:

$$A_V \sim \mathcal{N}_T(\mu_{A_V}, \sigma_{A_V}) = \frac{\mathcal{N}(\mu_{A_V}, \sigma_{A_V})}{1 - \Phi\left(-\frac{\mu_{A_V}}{\sigma_{A_V}}\right)}. \tag{B1}$$

Here, $\mathcal{N}$ is the standard normal distribution and $\Phi(x) = \frac{1}{2}\left(1 + \mathrm{erf}(x/\sqrt{2})\right)$ is the cumulative distribution function of $\mathcal{N}$. μ_{A_V} and σ_{A_V} are the mean and variance of the truncated normal distribution. Similar to Eq. 4, we allow μ_{A_V} and σ_{A_V} to depend on the physical properties of galaxies:

$$\mu_{A_V} = m_{\mu,1}(\log\ M_* - 10.) + m_{\mu,2}\log\ \mathrm{SFR} + c_\mu \tag{B2}$$

$$\sigma_{A_V} = m_{\sigma,1}(\log\ M_* - 10.) + m_{\sigma,2}\log\ \mathrm{SFR} + c_\sigma. \tag{B3}$$

The A_V distribution from our truncated normal (orange dashed) closely reproduces the observed SDSS A_V distribution (Figure 9). N_T is able to reproduce the overall skewness but unlike the slab model, it does not have a long high A_V tail. With more free parameters and a functional form that closely resembles the observed A_V distribution, the truncated normal model provides a flexible altnerative to the slab model and we include it in our analysis.
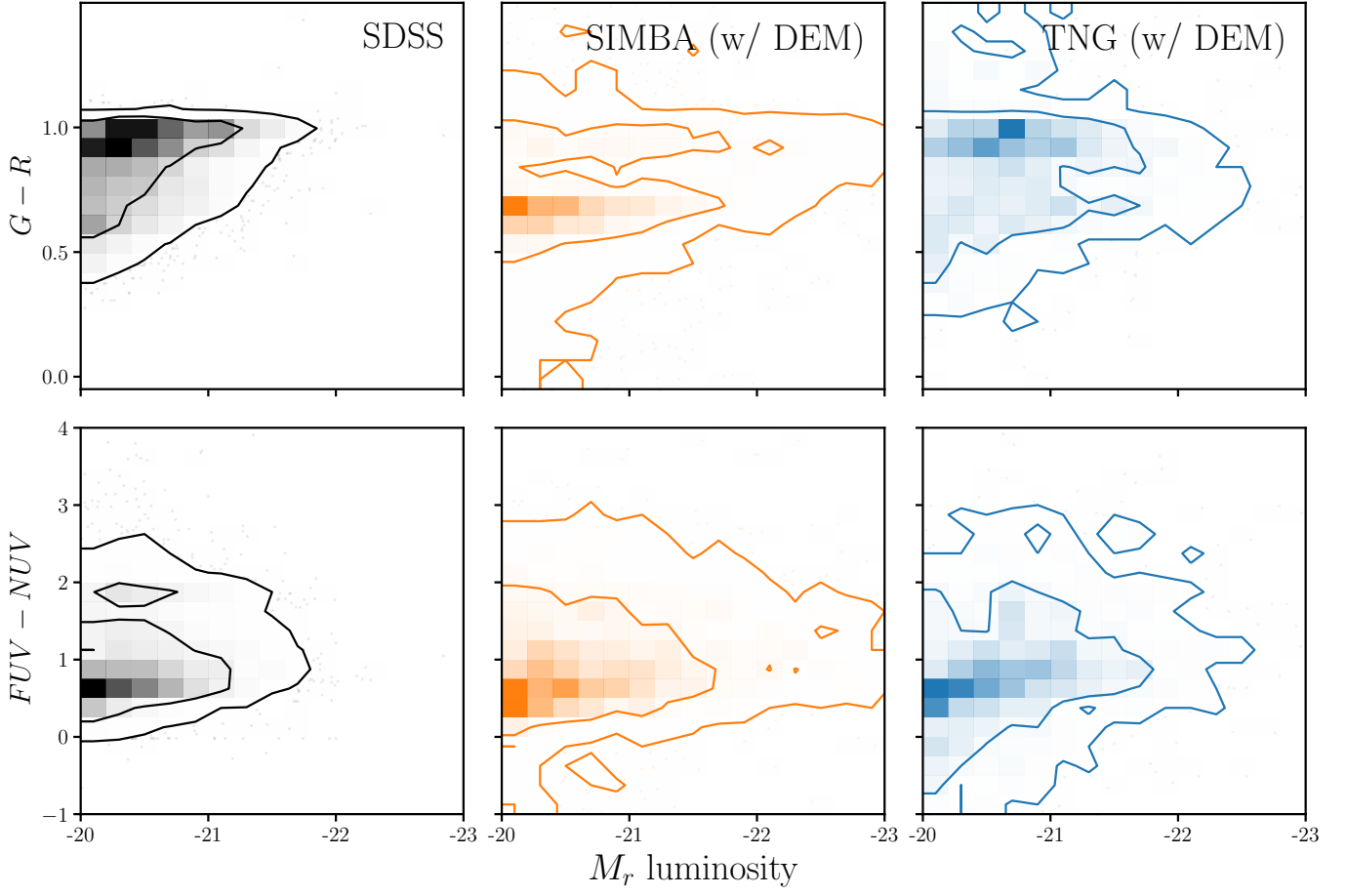
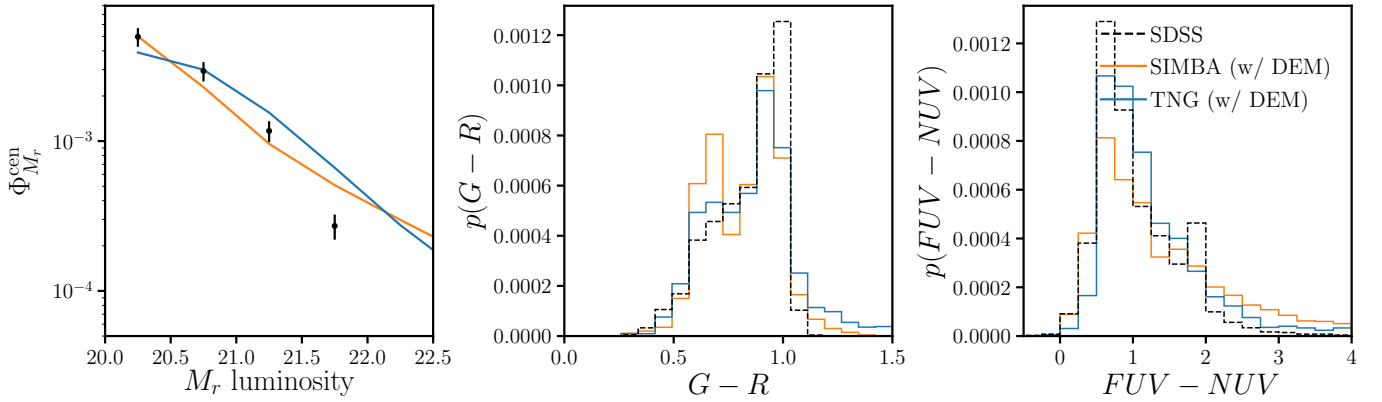**Figure 7.** Comparison of the observables predicted by the simulations with the posterior DEM.

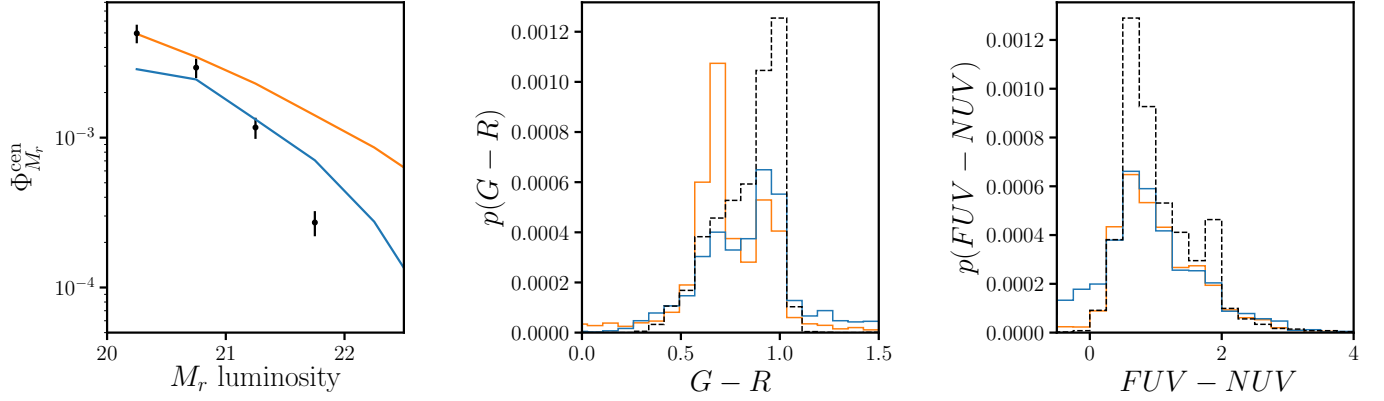**Figure 8.** Comparison of the observables predicted by the simulations with the posterior DEM.

Figure 9. Comparison of the observables predicted by the simulations with the posterior DEM.
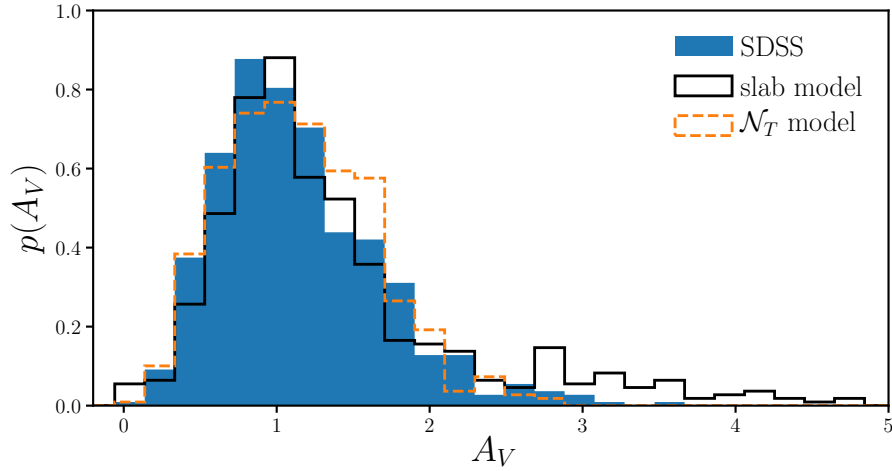

Figure 10. Comparison of A_V distribution of SDSS star-forming galaxies (blue) to predictions from the slab model (Eq. 3; black). detail on how SDSS SF galaxies are classified. The slab model assumes that there's a slab of dust in front of a galaxy. We use $\tau_V = 2$ for the slab model above. Regardless of τ_V, however, the slab model predicts a significantly more asymmetric and peaked A_V distribution than observations. Given this disagreement, *we include in our analysis a DEM with an empirical prescription for A_V based on a truncated normal distribution, which better reproduce the observed A_V distribution* (Section B).

REFERENCES

Abazajian K. N., et al., 2009, The Astrophysical Journal Supplement Series, 182, 543

Blanton M. R., Roweis S., 2007, The Astronomical Journal, 133, 734

Blanton M. R., et al., 2005, The Astronomical Journal, 129, 2562

Calzetti D., 2001, New Astronomy Reviews, 45, 601

Chabrier G., 2003, Publications of the Astronomical Society of the Pacific, 115, 763

Hahn C., Vakili M., Walsh K., Hearin A. P., Hogg D. W., Campbell D., 2017, Monthly Notices of the Royal Astronomical Society, 469, 2791

Ishida E. E. O., et al., 2015, Astronomy and Computing, 13, 1

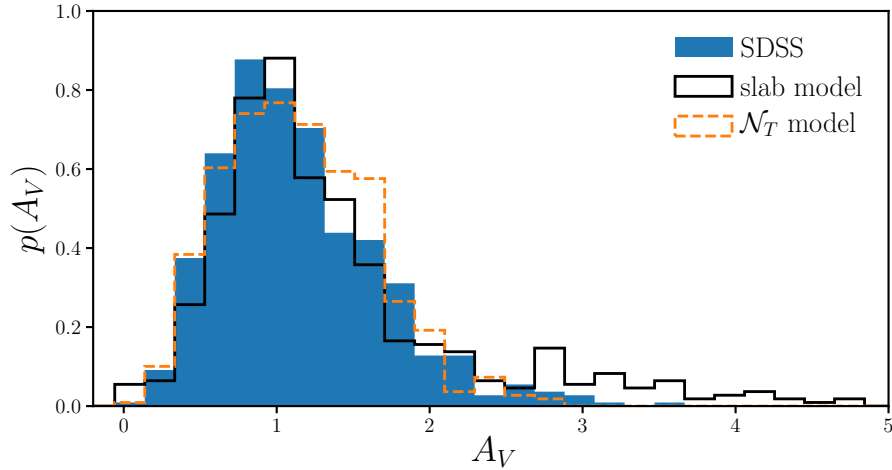Kriek M., Conroy C., 2013, The Astrophysical Journal Letters, 775, L16

Figure 11. Comparison of A_V distribution of SDSS star-forming galaxies (blue) to predictions from the slab model (Eq. 3; black). detail on how SDSS SF galaxies are classified. The slab model assumes that there's a slab of dust in front of a galaxy. We use $\tau_V = 2$ for the slab model above. Regardless of τ_V, however, the slab model predicts a significantly more asymmetric and peaked A_V distribution than observations. Given this disagreement, *we include in our analysis a DEM with an empirical prescription for A_V based on a truncated normal distribution, which better reproduce the observed A_V distribution* (Section B).

Narayanan D., Conroy C., Davé R., Johnson B. D., Popping G., 2018, The Astrophysical Journal, 869, 70

Noll S., Burgarella D., Giovannoli E., Buat V., Marcillac D., Muñoz-Mateos J. C., 2009, Astronomy and Astrophysics, 507, 1793

Salim S., Narayanan D., 2020, arXiv:2001.03181 [astro-ph]

Salim S., Boquien M., Lee J. C., 2018, The Astrophysical Journal, 859, 11

Somerville R. S., Primack J. R., 1999, Monthly Notices of the Royal Astronomical Society, 310, 1087

Somerville R. S., Gilmore R. C., Primack J. R., Domínguez A., 2012, Monthly Notices of the Royal Astronomical Society, 423, 1992

Tinker J., Wetzel A., Conroy C., 2011, preprint, 1107, arXiv:1107.5046

Tinker J. L., Hahn C., Mao Y.-Y., Wetzel A. R., Conroy C., 2018, Monthly Notices of the Royal Astronomical Society, 477, 935

Trayford J. W., Lagos C. d. P., Robotham A. S. G., Obreschkow D., 2020, Monthly Notices of the Royal Astronomical Society, 491, 3937

Tress M., et al., 2018, Monthly Notices of the Royal Astronomical Society, 475, 2363